Modelling and performance analysis of an absorption chiller with a microchannel membrane-based absorber using LiBr-H_2O, LiCl-H_2O and $LiNO_3$-NH_3

Mercedes de VEGA [1*], María VENEGAS [1,2], Néstor GARCÍA-HERNANDO [1]

* Corresponding author: E-mail address: mdevega@ing.uc3m.es
[1] ISE Research Group, Department of Thermal and Fluids Engineering, Universidad Carlos III de Madrid, Avda. Universidad 30, 28911 Leganés, Madrid, Spain
[2] GTA Research Group, Department of Thermal and Fluids Engineering, Universidad Carlos III de Madrid, Avda. Universidad 30, 28911 Leganés, Madrid, Spain

Abstract

In order to develop compact absorption refrigeration cycles driven by low heat sources, the simulated performance of a microchannel absorber of 5 cm length and 9.5 cm^3 in volume provided with a porous membrane is presented for three different solution-refrigerant pairs: LiBr-H_2O, LiCl-H_2O and $LiNO_3$-NH_3. The high absorption rates calculated for the three solutions lead to large cooling effect to absorber volume ratios: 625 kW/m^3 for the $LiNO_3$-NH_3, 552 kW/m^3 for the LiBr-H_2O and 318 kW/m^3 for the LiCl-H_2O solutions given the studied geometry. The performance of a complete absorption system is also analyzed varying the solution concentration, condensation temperature and desorption temperature. The $LiNO_3$-NH_3 and the LiBr-H_2O solutions provide the largest cooling effects. The $LiNO_3$-NH_3 can work at a lower temperature of the heating source, in comparison with the one needed in a LiBr-H_2O system. The lowest cooling effect and coefficient of performance are found for the LiCl-H_2O solution, but this mixture allows the use of lower temperature heating sources (below 70 ºC). These results can be used for the selection of the most suitable solution for a given cooling duty, depending on the available heat source and condensation temperature.

Keywords: absorption refrigeration; microchannel; membrane absorber; lithium bromide-water; lithium chloride-water; lithium nitrate-ammonia.

Nomenclature

A	area (m^2)
C	constant
C_p	specific heat ($kJ\ kg^{-1}\ K^{-1}$)
D	diffusion coefficient ($m^2\ s^{-1}$)
D_0	self-diffusion coefficient of ammonia ($m^2\ s^{-1}$)
D_e	diffusion term ($m^2\ s^{-1}$)
D_h	hydraulic diameter (m)
d_p	membrane pore diameter (m)
dz	discretisation length (m)

e height or thickness (m)
h convective heat transfer coefficient (W m^{-2} K^{-1})
i specific enthalpy (kJ kg^{-1})
J absorption rate (kg m^{-2} s^{-1})
k thermal conductivity (W K^{-1} m^{-1})
$\tilde{k}$ mass transfer coefficient (m s^{-1})
K mass transfer coefficient (kg Pa^{-1} m^{-2} s^{-1})
l width (m)
$\dot{m}$ mass flow rate (kg s^{-1})
M molecular weight (kg $mole^{-1}$)
Nu Nusselt number, $Nu = hD_h/k$
P pressure (Pa)
Pr Prandtl number, $Pr = \mu C_p/k$
q thermal power (W)
R mass transfer resistance (kg^{-1} Pa m^2 s)
Re Reynolds number, $Re = uD_h\rho/\mu$
r_{QV} ratio between cooling capacity and absorber volume
R_u universal gases constant (J $mole^{-1}$ K^{-1})
Sh Sherwood number, $Sh = KD_h/D$
T temperature (ºC)
u velocity (m s^{-1})
U global heat transfer coefficient (W m^{-2} K^{-1})
w power (W)
x absorbent mass fraction ($kg_{absorbent}$ kg_s^{-1})
z length (m)

Greek symbols

δ constant
ε porosity
μ viscosity (Pa s)
Ξ Ackermann factor
ρ density (kg m^{-3})
τ tortuosity
Φ heat transfer rate factor

Subscripts

A absorber
ave average
b boundary layer
C condenser
cw cooling water
D desorber

E	evaporator
in	inlet
lv	liquid-vapour
m	membrane
out	outlet
ov	overall
P	pump
ref	refrigerant
s	solution
sat	saturation
v	vapour
va	vapour absorbed

1. Introduction

Large scale absorption chillers have been widely used with lithium bromide-water ($LiBr-H_2O$) or water-ammonia (H_2O-NH_3) as absorbent-refrigerant pairs. The $LiBr-H_2O$ absorption refrigeration cycles have reasonable coefficient of performance for applications with evaporating temperatures above 0 ºC (air conditioning). For lower temperatures, the H_2O-NH_3 is used, but with lower performance. These working pairs present however some drawbacks as corrosion, crystallization and toxicity [1]. The need for better absorbent-refrigerant pairs to improve the system performance and the heat and mass transfer of the absorption chiller has become one focus of research [2].

Previous studies agree in that the lithium nitrate-ammonia ($LiNO_3-NH_3$) mixture is thermodynamically more attractive and can be the most suitable solution alternative to H_2O-NH_3 systems working in the same conditions [3-5]. Comparison of the performances of H_2O-NH_3 and $LiNO_3-NH_3$ absorption cycles suggests that the last one can achieve higher cooling capacities and better coefficients of performance [2,3,4,6,7]. Experimental prototypes have already attained reasonable good coefficients of performance in air-conditioning applications [8-12]. The use of a rectification column after the desorber is avoided as the salt is a non-volatile absorbent. This also reduces the machine weight and cost [3,6,10,11,13]. Moreover, solar driven absorption with $LiNO_3-NH_3$ would provide improved performance over the conventional units, because of the lower desorber temperatures which allow operation with simple, flat-plate, solar collectors [4,6,8,13,14].

Efforts have also been made to find optimal absorbent solutions trying to replace the $LiBr-H_2O$ system because of its corrosiveness to steel, low availability and relatively high cost [15]. The lithium chloride-water ($LiCl-H_2O$) working pair is readily available and environmentally friendly and can be suitable for moderate temperature applications [1,16,17]. Moreover, the $LiCl-H_2O$ working pair could be preferred over $LiBr-H_2O$ for reasons of cost and long-term stability [1,18].

Meanwhile, the interest for small-scale absorption chillers in buildings and dwellings air-conditioning appliances has also increased, coupled with the use of solar thermal systems as a way to reduce the electricity consumption in these applications [3,4]. The absorber is one of the most performance limiting [19] and volume demanding [20] component of absorption systems. The main challenge in designing and operating these devices is to maximize the mass transfer rate by getting as much interfacial area as possible, minimizing the overall size. This can be achieved using membrane contactors in microchannel heat exchangers. This new technology has already been considered for LiBr-H_2O and H_2O-NH_3 refrigerant-solution pairs. A review of membrane contactors applied in absorption refrigeration systems has been presented by Asfand and Bourouis [21]. The potential of the membrane absorption technology for volume and cost reduction of absorption refrigerators has been reported theoretically by Chen et al. [22] and experimentally by Schaal et al. [23] for an absorber using hollow fiber membranes and the H_2O-NH_3 solution. Ali and Schwerdt [20] studied the characteristics of membranes for the vapour absorption using the LiBr-H_2O solution and Ali [24] designed and investigated the performance of an absorber with hydrophobic membrane in case the chiller operates at different values of the cooling water temperatures. Yu et al. [25] have shown the importance of the reduction in the solution film thickness to obtain high absorption rates in membrane-based absorbers. Isfahani and Moghaddam [26] tested an absorber using the LiBr-H_2O solution and a super hydrophobic nanofibrous membrane obtaining an absorption rate of about 0.006 kg/m^{2}s, using channels of 100 μm thick and a flow velocity of 5 mm/s. Venegas et al. [27] developed a simple model to predict the performance of a LiBr-H_2O microchannel absorber operating with a microporous membrane. Recently, Asfand et al. [28] present a simulation of a membrane-based absorber with a quaternary salt system (LiBr+LiI+$LiNO_3$+LiCl) and a ternary mixture of alkali nitrates ($LiNO_3$+KNO_3+$NaNO_3$) with water as refrigerant using the ANSYS/FLUENT code.

The present paper is devoted to covering the two main issues reported above: scale down the size of absorption systems by means of a microchannel absorber, provided with a porous membrane, and study its performance with substitute absorbent-refrigerant pairs that have not been considered before in this kind of absorber. Our approach differs from the work of Asfand et al. [28] in that the mixtures evaluated and the dimensions of the microchannels used are different. Further, in the present work a simplified model (described in [27]) is used, which is less time consuming than the numerical codes and needs less hypotheses to simulate the system. The considered absorbent-refrigerant pairs are LiCl-H_2O and $LiNO_3$-NH_3, which have already been used in conventional absorbers, but not in membrane-based absorbers. Their performance in the membrane-based absorber is compared with the LiBr-H_2O solution. For the first time in relation to membrane-based absorbers, we provide the values of the cooling effect and coefficient of performance of a complete absorption system working with this kind of micro absorber. Additionally, the temperatures needed in the desorber are calculated for each of the solutions.

2. Microchannel absorber model

In the proposed absorber a microporous membrane provides the surface contact area between the vapour and the solution. The refrigerant vapour (in the present study water or ammonia) passes through the membrane and it is absorbed by the solution ($LiBr\text{-}H_2O$, $LiCl\text{-}H_2O$ or $LiNO_3\text{-}NH_3$) flowing inside constrained flow passages. The vapour pressure difference across the membrane is the driving force for vapour transfer. The heat of absorption is extracted by a cooling water stream, confined also in microchannels and separated from the solution by a metallic wall.

2.1. Microchannel absorber configuration

The configuration considered for the absorber in the present study is shown in Fig. 1(a). The dimensions of the microchannels are 150 μm height and 1.5 mm width. The length of the channels is 5 cm. We have considered a membrane 60 μm thick, with 0.8 porosity and a pore diameter of 1 μm. The number of water and solution channels is the same, equal to 13.

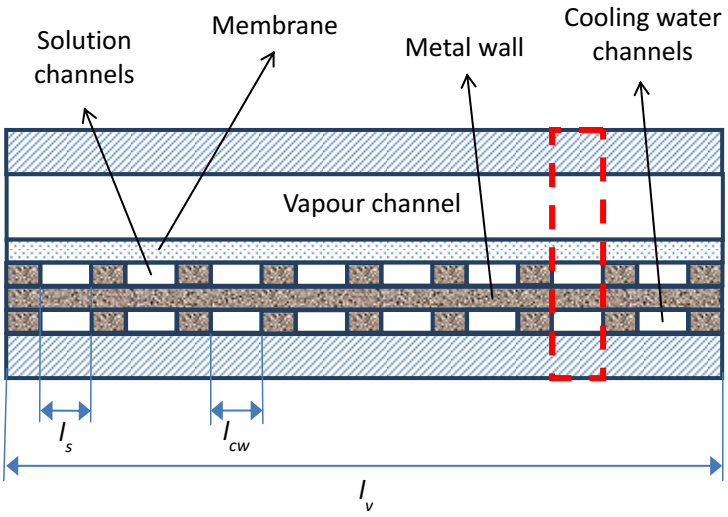

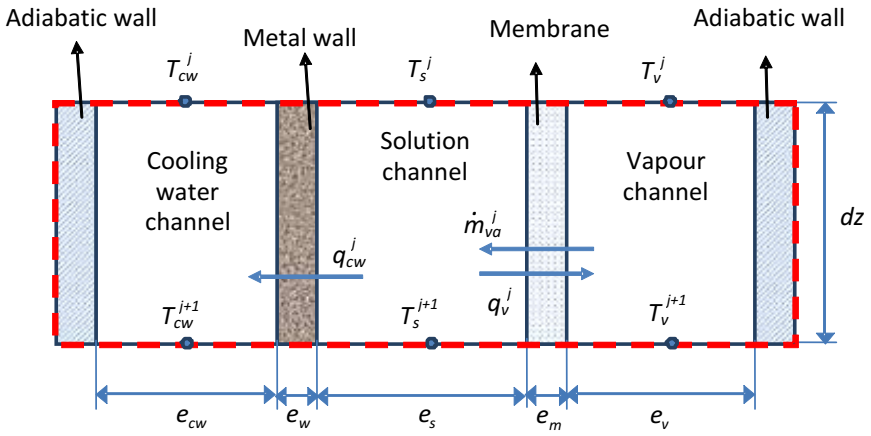

Fig. 1. (a) (Top): Microchannel absorber cross-section; (b) (Bottom) Differential control volume for heat and mass transfer balances.

2.2. Heat and mass transfer model

Our model is based in the dusty-gas model for the vapour mass transfer through the membrane and the film theory: the heat and mass transfer equations are described in terms of the corresponding mass and heat transfer coefficients. In the following paragraphs, an overview of the modelling approach is provided. For a detailed discussion of the complete procedure and the correlations employed, the reader is referred to our previous publication (Venegas et al. [27]) because the same modelling approach is used in the present work.

The microchannel absorber is divided in differential elements, as shown in Fig. 1(b), where mass and energy balances are sequentially applied.

2.2.1. Heat transfer

The energy balance applied to the differential element *j*, of length *dz* in Fig. 1(b), is written as:

$$(\dot{m}_{va} i_{lv})^j = (\dot{m}\cdot i)_s^{j+1} - (\dot{m}\cdot i)_s^j + (\dot{m}\cdot i)_v^{j+1} - (\dot{m}\cdot i)_v^j + \dot{m}_{cw} Cp_{cw}^j \left(T_{cw}^{j+1} - T_{cw}^j\right) \quad (1)$$

Left term in Eq. (1) corresponds to the thermal power released during the absorption of the vapour flow rate $\dot{m}_{va}$ into the solution. This heat is transferred to the solution, vapour and cooling water. The heat transfer between the solution and the cooling water, considering the last one as incompressible liquid with constant specific heat, can also be written as in Eq. (2):

$$\dot{m}_{cw} Cp_{cw}^j \left(T_{cw}^{j+1} - T_{cw}^j\right) = U_{s\_cw}^j A \left(T_s^j - T_{cw}^j\right) \quad (2)$$

In the same way, the heat transfer between the solution and the vapour can be expressed as in Eq. (3):

$$(\dot{m}\cdot i)_v^{j+1} - (\dot{m}\cdot i)_v^j = U_{s\_v}^j A \left(T_s^j - T_v^j\right) \quad (3)$$

The global heat transfer coefficients in Eqs. (2) and (3) are calculated by means of Eqs. (4) and (5):

$$\frac{1}{U^j_{s\_cw}} = \frac{1}{h^j_{cw}} + \frac{e_w}{k^j_w} + \frac{1}{h^j_{s,cw*}} \quad (4)$$

$$\frac{1}{U^j_{s\_v}} = \frac{1}{h^j_v} + \frac{e_m}{k^j_{m,ave}} + \frac{1}{h^j_{s,v*}} \quad (5)$$

The heat transfer coefficients (h) appearing in the overall coefficients U_{s_cw} and U_{s_v} in Eqs. (4) and (5) are estimated using heat transfer correlations taken from the literature. In the present study, we use the heat transfer correlations of Lee and Garimella [29] for the thermal entrance region and Shah and London [30] for fully developed flow, as described in [27]. These correlations take the form shown in Eqs. (6) and (7), respectively, where the Nusselt number for the fully developed flow is a constant, for the aspect ratio of the channels fixed with the dimensions specified in Section 2.1.

$$Nu^j = f(z, Re, Pr, D_h) = \frac{1}{C_1\left(z/_{RePrD_h}\right)^{C_2} + C_3} + C_4 \quad \text{(thermal entrance region)} \quad (6)$$

$$Nu^j = constant \quad \text{(fully developed flow)} \quad (7)$$

The aspect ratios and hydraulic diameters used in the present study are included in the validity ranges of the Lee and Garimella's correlation. Developed for laminar flow, condition that applies in the present work, the correlation of Shah and London has been previously used by some authors to predict the heat transfer performance in similar geometries of rectangular microchannels [31,32].

In the case of the solution channel, the effect of mass transfer on heat transfer is taken into account using modified heat transfer coefficients. Modified coefficients are found multiplying those obtained from Eqs. (6) and (7) by the Ackermann factor (Taylor and Krishna [33]) calculated as in Eq. (8):

$$\Xi = \frac{\Phi}{e^{\Phi}-1} \quad (8)$$

where the heat transfer rate factor Φ is defined as in [33]:

$$\Phi = J \cdot Cp_v \cdot e_s / k_v \quad (9)$$

In Eq. (9), J is the absorption rate, Cp_v and k_v are the vapour specific heat and conductivity, and e_s is the channel solution height.

The average thermal conductivity of the membrane, $k_{m,ave}$ in Eq. (5), is calculated using the equation given by Martínez and Rodríguez-Maroto [34]:

$$k_{m,ave} = \varepsilon k_v + (1-\varepsilon) k_m \quad (10)$$

In Eq. (10), k_v is the thermal conductivity of the vapour inside the membrane pores, while k_m is the thermal conductivity of the membrane solid material. The thermal conductivity of the membrane is taken equal to 0.22 W/mK, the same used by Ali [24].

2.2.2. Mass transfer

The conservation of mass in each differential element relates the solution ($\dot{m}_s$) and vapour ($\dot{m}_v$) mass flow rates and the mass fraction of the absorbent (x) in the solution are calculated with Eqs. (11) to (13):

$$\dot{m}_s^{j+1} = \dot{m}_s^j + \dot{m}_{va}^j \quad (11)$$

$$\dot{m}_v^{j+1} = \dot{m}_v^j - \dot{m}_{va}^j \quad (12)$$

$$x^{j+1} = x^{j} \frac{\dot{m}_s^j}{\dot{m}_s^{j+1}} \quad (13)$$

The mass flow rate of vapour transported across the membrane ($\dot{m}_{va}$) in Eqs. (11) and (12) is calculated taking into account the conditions of the bulk vapour and bulk solution streams. Eq. (14) provides, for the differential element *j*, the absorbed vapour mass flow rate:

$$\dot{m}_{va}^j = J^j \cdot A \quad (14)$$

where *A* is the heat and mass transfer area. The absorption rate is calculated as:

$$J^j = \frac{P_v - P_s^j}{R_{ov}^j} \quad (15)$$

In Eq. (15), P_v is the bulk vapour pressure and P_s is the refrigerant vapour partial pressure (water or ammonia) corresponding to the bulk solution concentration and temperature. The overall mass transfer resistance between the vapour and bulk solution (R_{ov}) includes the resistance to diffusion through the solution boundary layer (R_b) and the resistance to diffusion of vapour through the membrane active layer (R_m). The same approach presented by Ali [24] and applied in Venegas et al. [27] is followed here to obtain the overall mass transfer resistance:

$$R_{ov} = R_b + R_m = \frac{1}{K_b} + \frac{1}{K_m} = \frac{P_{sat}^j}{\rho_{ref}^j \tilde{k}_s^j} + \left[\frac{M}{e_m}\left(\frac{D_e}{R_u T_m}\right)\right]^{-1} \quad (16)$$

On the right side of Eq. (16), P_{sat} is the refrigerant saturated pressure corresponding to the bulk solution temperature, ρ_{ref} is the liquid refrigerant density and $\tilde{k}_s$ is the mass transfer coefficient between the solution-vapour interface and the bulk solution. A suitable correlation for mass transfer in microchannels has not been found in the open literature. For this reason, the mass transfer coefficient of the solution $\tilde{k}_s$ is calculated as in Eq. (17) using mass and heat transfer analogy, using the definition of Sherwood number:

$$\tilde{k}_s^j = \frac{Sh_s^j D^j}{D_h} \quad (17)$$

In Eq. (17), *D* is the diffusion coefficient for each of the absorbent-refrigerant pairs considered in this study and D_h is the hydraulic diameter. The Sherwood number, Sh_s, is obtained by means of the same correlations used to evaluate *Nu* for the heat transfer problem, Eqs. (6) and (7), replacing the Prandlt number by the Schmidt number, as in Eq. (18):

$$Sh_s{}^j = f(z, Re, Sc, D_h) = \frac{1}{C_1\left(z/ReScD_h\right)^{C_2} + C_3} + C_4 \quad (18)$$

This heat and mass transfer analogy has already been used in previous works, for similar problems [24,35].

The last term in Eq. (16) corresponds to free molecular flow through the membrane. It is a function of the molecular weight of the vapour, *M*, the membrane thickness, e_m, and the temperature of the membrane, T_m. Eq. (19) provides the diffusion term, D_e, as a function of the porosity, ε, pore diameter, d_p, and tortuosity, τ, of the membrane as in [27]:

$$D_e = \frac{\varepsilon d_p}{3\tau}\left(\frac{8R_u T_m}{\pi M}\right)^{0.5} \quad (19)$$

The temperatures and concentration along the channels cannot be explicitly determined from equations (1) to (19). Therefore, the above set of equations has been solved iteratively (in less than 30 seconds) using Engineering Equation Solver software, EES™. The advantage of the present model is that, besides its simplicity, it considers that temperatures and concentration are changing along both zones: thermal entrance region and fully developed flow. Additionally, the influence of mass transfer on heat transfer, which has not been included before in similar investigations using these solutions, is taken into account.

2.3. Fluid properties

Special care has been taken to select or obtain the correlations for the diffusion coefficient of the refrigerants into the solutions. The different sources used to predict the properties are described in the following paragraphs for the three solutions.

The thermodynamic and physical properties of the LiBr-H_2O solution have been calculated using the functions provided by EES based on [36-38].

According to Fig. 2(a), the diffusion coefficient of water in the LiBr-H_2O reported by Kim et al. [39] agrees well (differences are below 20%) with the Mittermaier et al. [40] correlation, which is the expression used in the present simulation.

The density, specific heat and thermodynamic properties of the LiCl-H_2O pair have also been calculated using the functions of EES, based on [41]. The viscosity and thermal conductivity have been predicted by means of the correlations provided by Conde [42].

In Fig. 2(a) the data reported by Kim et al. [39] for the diffusion coefficient of water into the LiCl-H_2O solution and the values obtained with the correlation of Conde [43], are plotted with data also reported by Bouazizi and Nasr [44] for the same solution. The differences between the data found in the open literature and the correlation of Conde [43] are below 10%. Therefore, in the present study this correlation is used in the simulation for the LiCl-H_2O mixture.

In the case of the $LiNO_3$-NH_3 solution, the thermodynamic and physical properties have been calculated according to the correlations proposed by Libotean et al. [45,46]. The diffusion coefficient of ammonia into the solution is calculated using Eq. (20), specifically developed in the present work:

$$D = D_0\left\{1 - \left[1 + \left(\frac{\sqrt{x_{LiNO_3}}}{\delta_1}\right)^{\delta_2}\right]^{\delta_3}\right\} \quad (20)$$

where $\delta_1 = 0.524$, $\delta_2 = -6.65$, $\delta_3 = -0.95$ and D_0 is the self-diffusion coefficient of ammonia.

This equation relates the data provided by Infante Ferreira [47] in an equation of a similar form to the one proposed by Conde [43] for the LiCl-H_2O solution. In Fig. 2 (b),

the results of this function is plotted with the data referred in Kusaka et al. [48] and also the data provided by Infante Ferreira [47].

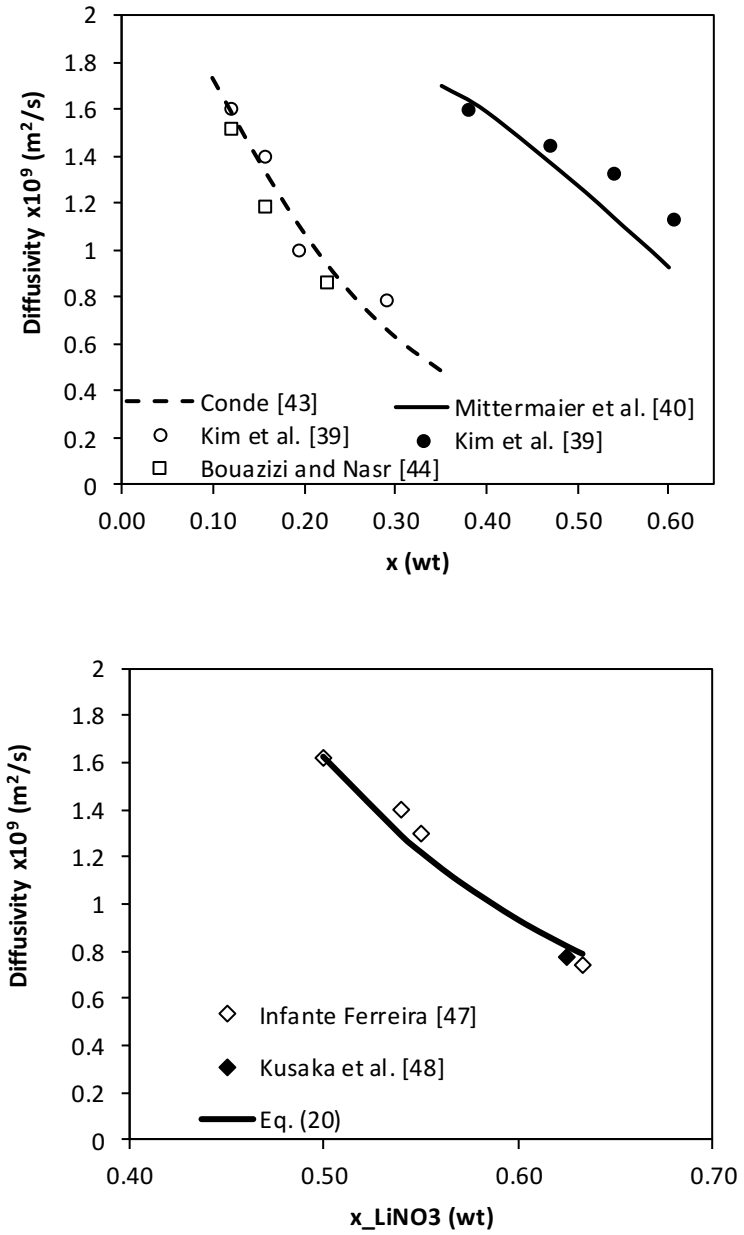

Fig. 2. Diffusion coefficients: (a) (Top) water into LiBr-H_2O (bold) and LiCl-H_2O (dashes and unbold); (b) (Bottom) ammonia into $LiNO_3$-NH_3 solution.

3. Results and discussion

The main objective of our paper is to derive the theoretical performance data of a membrane-based absorber integrated in a complete absorption chiller. The model is capable of comparing the heat and mass transfer behaviour along the channels for the LiBr-H_2O solution and the less conventional $LiNO_3$-NH_3 and LiCl-H_2O mixtures.

3.1. Model validation

The current model has been validated with experimental data obtained by Isfahani and Moghaddam [26] with the LiBr-H_2O solution. No experimental data of the two other solutions have been found in the open literature using membrane-based absorbers, but correlations used in the present model remain valid in all the cases. As stated by Herold et al. [49], the mass transfer process controls the coupled heat and mass transfer in the absorber and therefore validation has been performed comparing the absorption rate predicted with the experimental data reported by Isfahani and Moghaddam [26]. In the experimental case, the solution and cooling water channels measure 1 and 4 mm in width respectively. The cooling water channel height was 0.4 mm. The solution channel of 0.16 mm height was used for the validation.

Fig. 3 shows a comparison between the absorption rate predicted by the model, using the data of Isfahani and Moghaddam [26], and their experimental results. The figure shows the influence of the vapour pressure and the cooling water inlet temperature on the absorption rate. Experiments and simulation agree well. Fig. 3(a) shows the good prediction of the model concerning the vapour pressure influence. The absorption rate increases because the vapour pressure potential rises. In the case of Fig. 3(b), the increase in the cooling water inlet temperature reduces the driving force for heat transfer between the solution and the cooling water, leading to an increase of the solution temperature. Consequently, the solution water vapour pressure increases, which reduces the vapour pressure potential for mass transfer. The mean absolute error of the model predictions respect to all experimental data represented in Fig. 3 is 9.4%. This low difference demonstrates the value of the model to perform a good prediction of the membrane-based absorber performance.

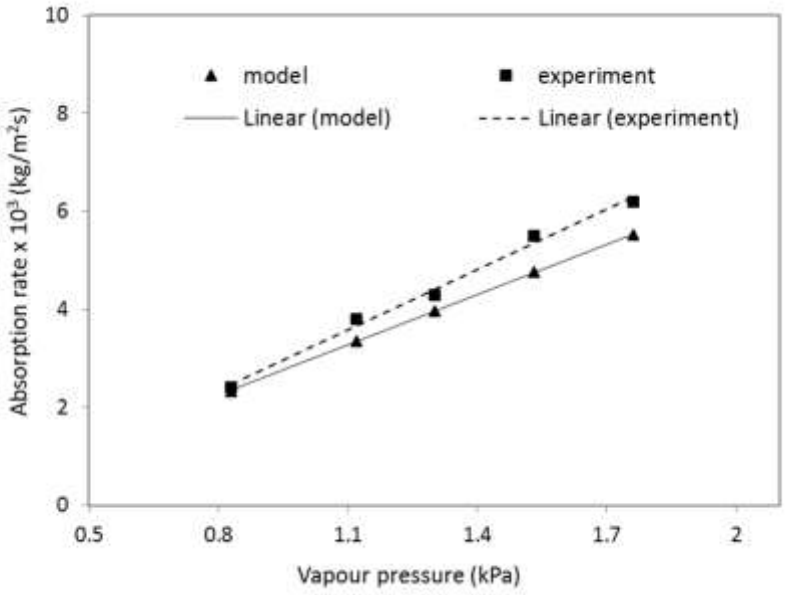

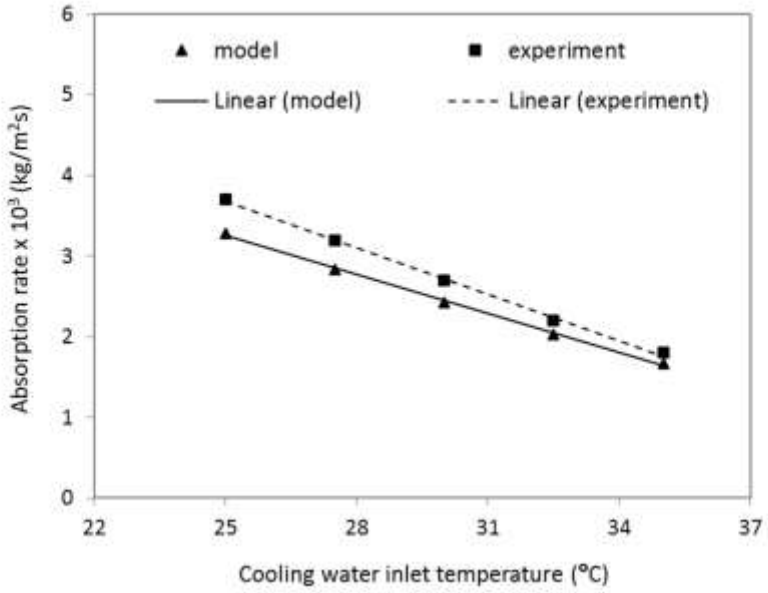

Fig. 3. Absorption rate as a function of (a) (Top): the vapour pressure; (b) (Bottom) the cooling water inlet temperature. Comparison between model and experimental results of Isfahni and Moghaddam [26].

3.2. Mass and heat transfer along the channels

The performance of the membrane-based micro absorber, working with the three different solutions, is evaluated in the following paragraphs. We have used as input parameters: concentration, inlet solution and cooling water temperatures, absorber vapour pressure and solution mass flow rate (represented by the solution Reynolds number along the channels), as shown in Table 1. These data represent typical operating conditions of single-stage absorption chillers and are similar to those used by Kim et al. [39] for the LiBr-H_2O solution and Hernández-Magallanes et al. [10] for the $LiNO_3$-NH_3 solution. Data for the LiCl-H_2O mixture approach the optimal values found by Bellos et al. [50] for a solar absorption cooling system and they correspond also to the ones employed in Kim et al. [51]. If compared to the LiBr-H_2O solution, the lower concentration used is related to the higher crystallization possibility.

Table 1. Input parameters used for the simulation of the absorber.

	LiBr-H_2O	LiCl-H_2O	$LiNO_3$-NH_3
Absorbent mass fraction at the inlet (%)	60	44	51.6
Inlet solution temperature (ºC)	40	35	40
Inlet cooling water temperature (ºC)	30	30	30
Solution Reynolds number	60	60	60
Vapour temperature (ºC)	7.5	7.5	7.5

The mass transfer resistance between the solution-vapour interface and the bulk solution Rb and the membrane mass transfer resistance Rm are represented in Fig. 4 for the three mixtures along the channels. For the three solutions, the membrane mass transfer resistance Rm remains almost constant taking the values of $9.62.10^4$ Pa kg^{-1} m^2 s for the LiBr-H_2O case, $9.52.\ 10^4$ Pa kg^{-1} m^2 s for the LiCl-H_2O mixture and $9.9.\ 10^4$ Pa kg^{-1} m^2 s for the $LiNO_3$-NH_3 solution. As discussed by Ali and Schwerdt [20] and shown in Berdasco et al. [35], membrane resistance is mainly controlled by the maximum pore diameter allowable to avoid penetration of the solution into the membrane pores. In our case, the pore diameter is relatively large, 1 μm, giving a membrane mass transfer resistance that for the $LiNO_3$-NH_3 solution is negligible, when compared to the bulk resistance (as also occurred in Berdasco et al. [35]). The higher bulk resistance obtained using the $LiNO_3$-NH_3 solution is due to the higher saturation pressure of ammonia in comparison to water for the same refrigerant temperature, according to Eq. (16). In the case of the aqueous solutions the relative importance of both resistances is very similar, and the behaviour of the LiBr-H_2O and LiCl-H_2O solutions is as the one already discussed in Venegas et al. [27].

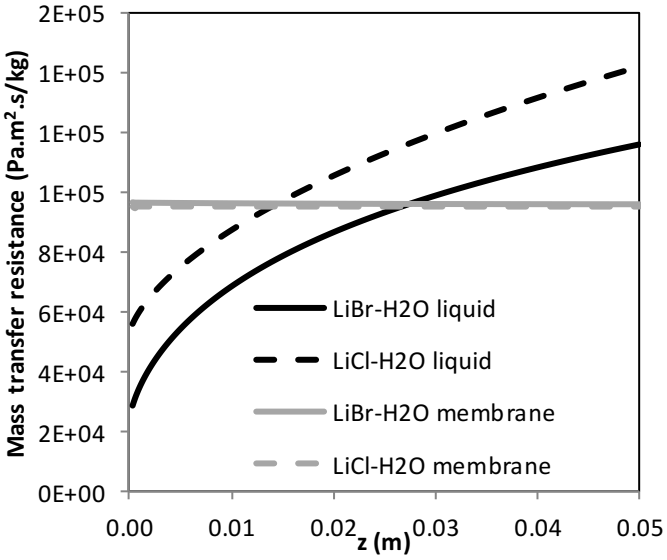

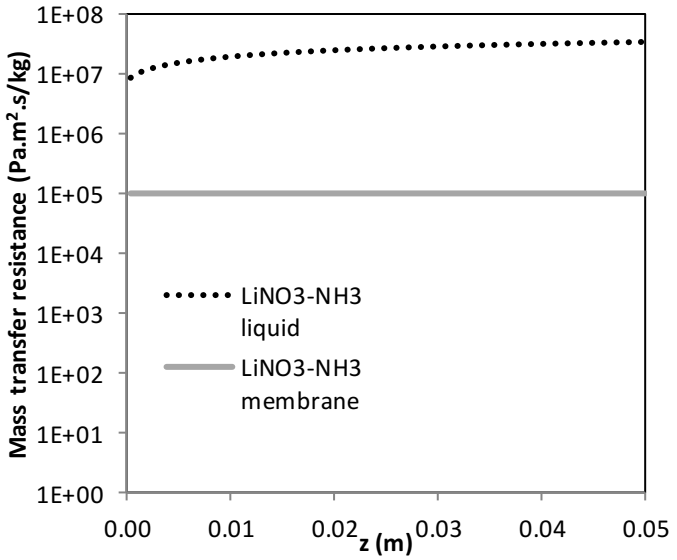

Fig. 4. Solution and membrane mass transfer resistances along the channels: (a) (Top) H_2O as refrigerant and (b) (Bottom) NH_3 as refrigerant.

The absorption rate along the channels is represented in Fig. 5. For the three solutions (and mainly for $LiNO_3$-NH_3), at the channels entrance, when higher pressure potential and mass transfer coefficient are available, the mass transfer rates are higher. The absorption rates decrease as the solutions heat, absorbing vapour along the channels. The higher driving potential provided by the working vapour pressures of the $LiNO_3$-NH_3 leads to higher mass transfer rates. The LiCl-H_2O solution presents a lower absorption rate than the LiBr-H_2O pair because of the lower driving potential and lower diffusivity of the vapour into the solution.

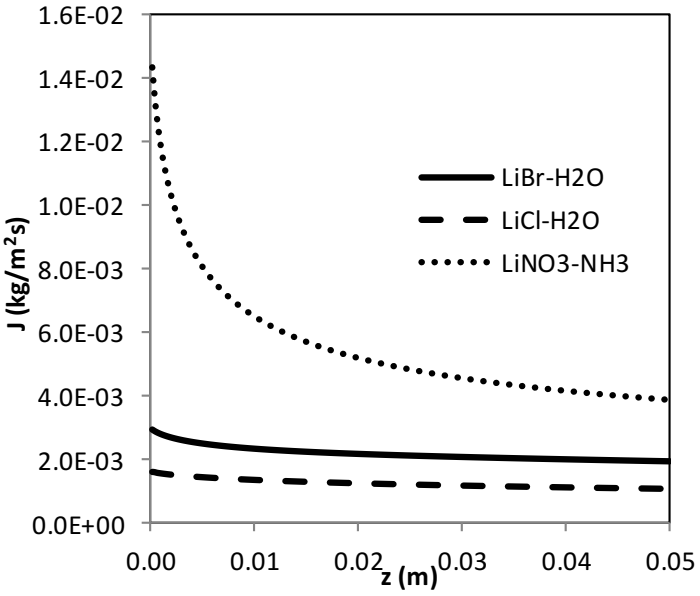

Fig. 5. Absorption rate along the channels.

Very high heat transfer coefficients are predicted in the present study for the three solutions, as shown in Fig. 6. The strong decrease observed in the figure for the convection coefficients corresponds to the change from thermal entrance region to fully developed flow. Additionally, in the fully developed flow region, as the aspect ratio of the channels is constant, the convection coefficient is also constant (see Eq. (7)). On the other hand, the higher values of the Prandtl number for the LiCl-H_2O pair provide higher values of the heat transfer coefficient for this solution. The fully developed flow is reached first in the LiBr-H_2O case, while it appears later for the LiCl-H_2O.

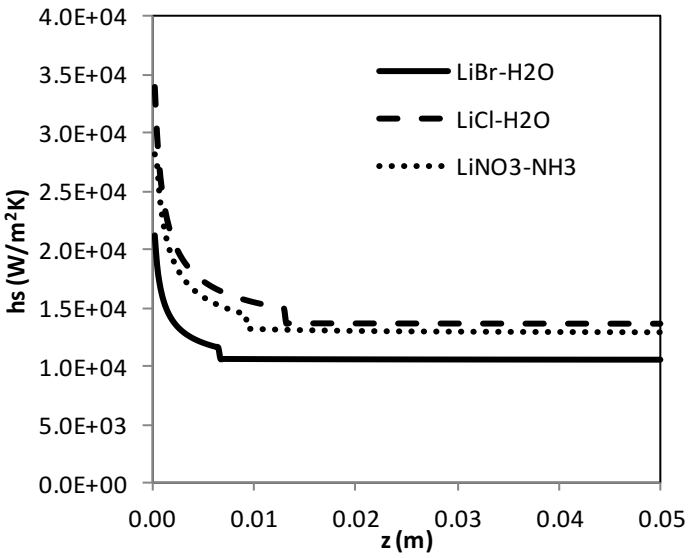

Fig. 6. Solution heat transfer coefficient along the channels.

The cooling power of an absorption chiller equipped with the absorber modelled in the present work and the ratio between this cooling power and the absorber volume, r_{QV}, along the channels, are shown in Fig. 7. The cooling power is represented in Fig. 7(a). This is the integrated value obtained for the different lengths shown. The cooling power is calculated taking into account the vaporization enthalpy of the refrigerant at the absorber pressure and the mass flow rate of vapour absorbed by the solution in the membrane-based absorber. The higher absorption rates provided by the $LiNO_3$-NH_3 solution leads to higher refrigeration rates, while the lower mass transfer rates obtained using the LiCl-H_2O pair cause the lowest values reached in the cooling power.

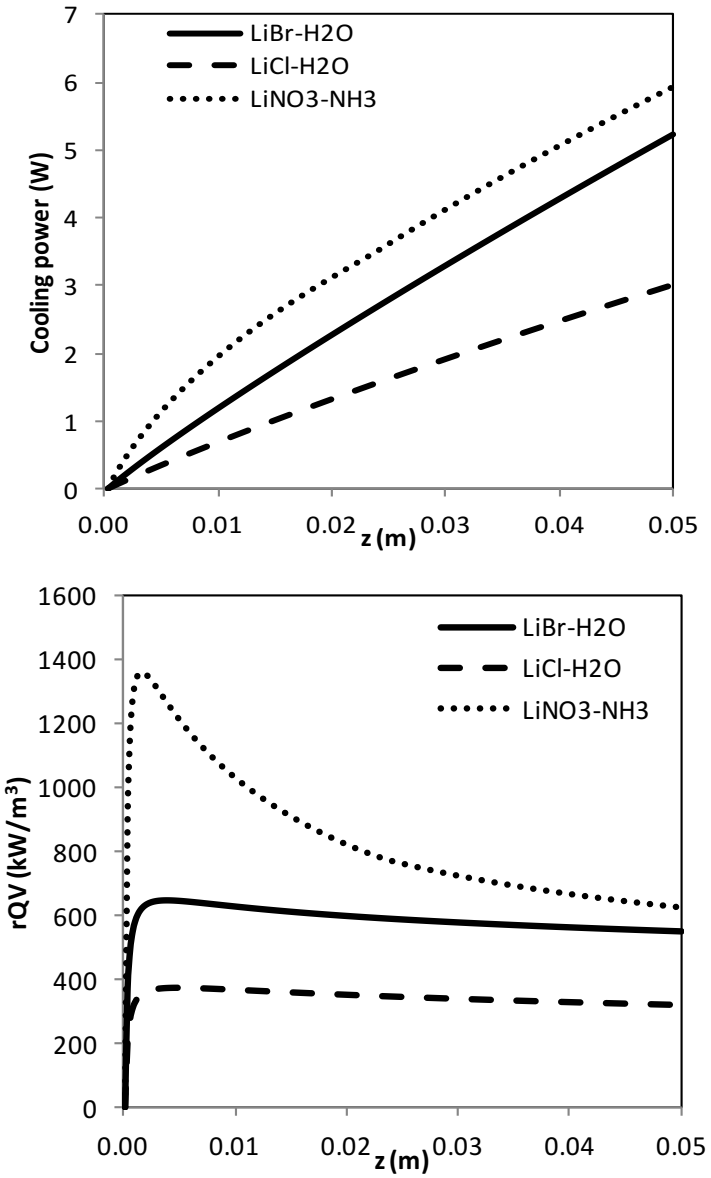

Fig. 7. (a) (Top) Cooling power; (b) (Bottom) Ratio of cooling power to absorber volume, r_{QV}, as a function of the channel length

The ratio between the cooling power and the absorber volume, r_{QV} can be used to select the proper channel length and solution in order to minimize the absorber size. In Fig. 7(b), the ratio suddenly increases with the channel length, reaching its maximum value at approximately 3 mm length. From this point, the ratio decreases. The high values observed at the channel entrance are associated to the high heat and mass transfer coefficients and the higher pressure potential at the inlet of the absorber. As these coefficients decrease when the channel length increases, the quantity of vapour absorbed decreases along the channel. Hence, in order to optimize the absorber size, when designing the absorber, it is not recommended to use very long channels, because the increase of the absorber size is higher than the increment obtained in the cooling power. This is an important conclusion derived from the results of the present work.

For the present case, the r_{QV} values obtained using an absorber of 5 cm length, are 625, 552 and 318 kW/m^3 for the $LiNO_3$-NH_3, LiBr-H_2O and LiCl-H_2O solutions, respectively. For the sake of comparison, some r_{QV} values obtained using conventional absorbers have been retrieved from the open literature. For example, using LiBr-H_2O, r_{QV} is in the order of 450 kW/m^3 in conventional and marketed shell and tubes falling film absorbers [27]. Kim et al. [51] in an experimental falling film absorber, constructed of two concentric tubes and working with LiCl-H_2O, obtained an r_{QV} in the order of 50 kW/m^3. In [10], a falling film absorber of 25.4 cm in diameter and a height of 70 cm was tested in a $LiNO_3$-NH_3 cooling system of 1.5 kW of cooling capacity, leading to a ratio of cooling to absorber volume in the order of 40 kW/m^3. The LiBr-H_2O technology is extensively and commercially available. As a well stablished technology, the LiBr-H_2O falling film absorber configuration is probably at present more optimized than the configuration for the much less employed $LiNO_3$ and LiCl solutions. For this reason, the volume ratios obtained in this work for the $LiNO_3$-NH_3 and LiCl-H_2O systems seem very high, respect to the experimental values using falling absorbers, when compared to the ratio for the LiBr system.

From the comparison between the r_{QV} results obtained using conventional and membrane-based absorbers, it can be concluded that smaller absorbers can be used employing membrane technology. Due to these reduced dimensions, these absorbers are specially suggested for low to medium cooling loads applications (as the ones found in households). The $LiNO_3$-NH_3 solution, considering compactness, is specially recommended, because of the smaller size of this system. This conclusion is a novelty of the present paper regarding the selection of the solution to be used in membrane-based absorbers. Moreover, the modular design of this type of heat and mass exchanger can easily provide a proper scale up, which could allow even higher cooling effect to absorber volume ratios. For example, it could be easy to increase the capacity in such a way that the vapour and cooling water channels are shared by adjacent modules. In this way, this ratio can be increased almost twice. As a general rule, microchannel heat exchangers have low material costs. In conventional LiBr-H_2O shell and tube absorbers, the cooling to volume ratio is 450 kW/m^3. According to our previous parametric study (Venegas et al. [27]) the optimization of this parameter provides a maximum ratio for the LiBr-H_2O microchannel absorber equal to 1090 kW/m^3 yielding to a reduction in volume for a given cooling duty that can be more than twice in comparison to a falling film absorber, with the proportional reduction in raw material. Considering the membrane, its cost is low, ranging from 0.04 to 0.13 USD/cm^2. While the application of microchannel heat exchangers in industry has been slowed by high manufacturing costs, at present, there is an intensive work toward low-cost fabrication technologies. Alternate processes for the production of microchannel devices are under study and exploring the cost structure of high volume manufacturing approaches will certainly lower cost fabrication [52,53].

Previous results of mass transfer coefficient, absorption rate, heat transfer coefficient, cooling power and ratio between cooling power and absorber volume have not been found in the open literature up to now for the $LiCl\text{-}H_2O$ and $LiNO_3\text{-}NH_3$ solutions related to microchannel membrane-based absorption technology.

3.3. Absorption chiller performance

As stated in the introduction, one of the interests of the alternative solutions ($LiCl\text{-}H_2O$ and $LiNO_3\text{-}NH_3$) is the possibility of working in systems supplied with solar thermal energy or, more generally, in applications where the desorber is fed with low heating temperatures. In order to evaluate the possible working conditions considering the complete absorption system, for an evaporation temperature of 7.5 ºC, the absorber has been studied operating in a complete absorption system as the one represented in Fig. 8.

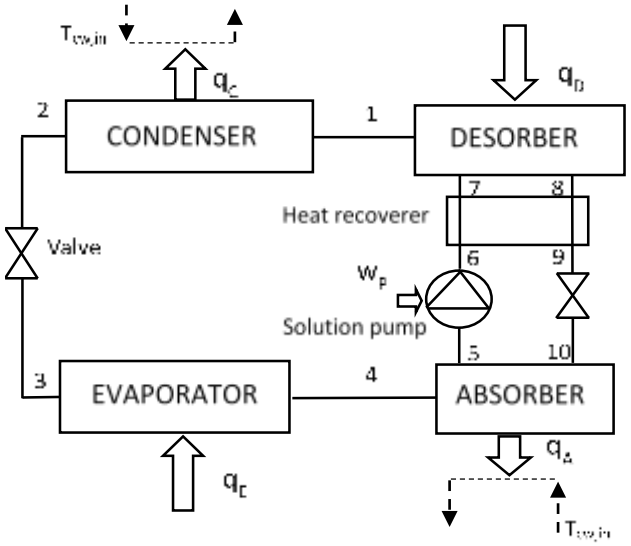

Fig. 8. Absorption chiller.

The theoretical approach followed for the analysis of the complete system is shown in Fig. 9. Once equations for the absorber are solved, energy and mass conservation equations are applied for each of the components. The model assumptions include no thermal losses to the surrounding from the components; the solution leaving the generator is saturated; the vapour leaving the evaporator and the liquid leaving the condenser are assumed to be saturated, and the vapour and the solution leaving the generator are at the same temperature. The condenser and the absorber are subjected to the same cooling medium, and we assume that the solution leaving the absorber and the liquid leaving the condenser are at the same temperature, as in [4,16].

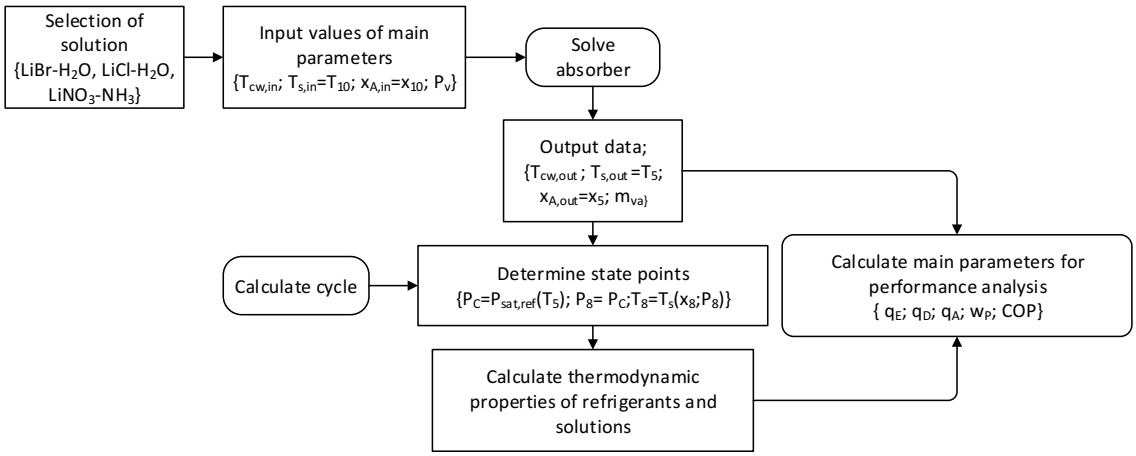

Fig. 9. Flow chart of the cycle simulation.

Different inlet solution concentrations and temperatures have been considered. The range of concentrations and solution inlet temperatures for the comparison of the LiBr-H_2O and LiCl-H_2O cases are the same ones used by Kim et al. [51]. For the comparison of the $LiNO_3$-NH_3 working pair, the values of the solution concentration and temperature are in the range of the ones reported by Hernández-Magallanes et al. [10]. The absorbent concentration is limited to avoid crystallization. These conditions are summarized in Table 2. Up to the authors' knowledge, no previous studies are available evaluating the effect of these variables on the cycle performance using the $LiNO_3$-NH_3 and LiCl-H_2O pairs using membrane-based absorbers.

Table 2. Input parameters used for the simulation of the absorption chiller.

Parameter	LiBr-H_2O	LiCl-H_2O	$LiNO_3$-NH_3
Vapour pressure, P_v (kPa)	1	1	564
Solution inlet temperature, T_{10} (ºC)	35-42	33-37	35-42
Vapour inlet temperature, T_v (ºC)	7.5	7.5	7.5
Inlet cooling water temperature, $T_{cw,in}$ (ºC)	30	30	30
Solution inlet concentration, x_{10} (%)	57-60	41-44	48-51.6

The cooling effect and the coefficient of performance, COP, for a solution inlet temperature of 35 ºC (and a temperature of the cooling water of 30 ºC), varying the solution concentration, are presented in Figs. 10 and 11.

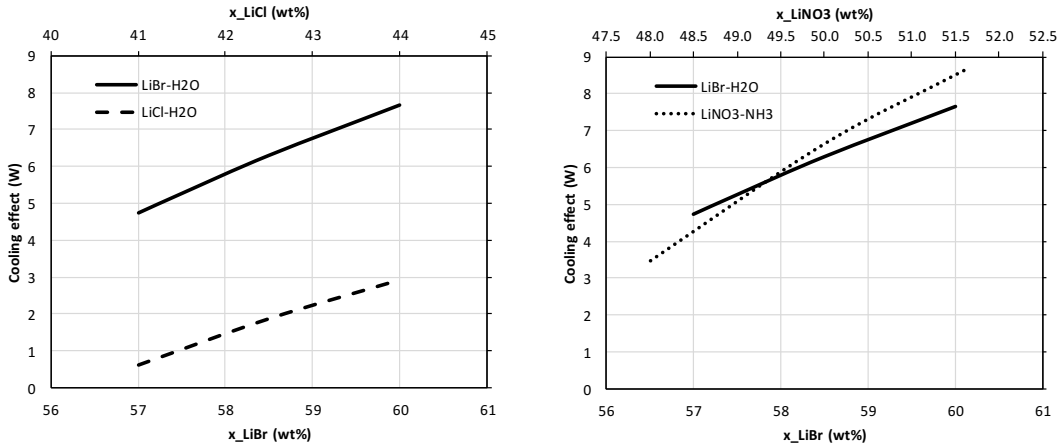

Fig. 10. Effect of solution concentration in the cooling effect of an absorption chiller working with a 5 cm long membrane absorber: LiCl-H_2O and LiBr-H_2O (a)(left); $LiNO_3$-NH_3 and LiBr-H_2O (b)(right).

The lowest cooling effect is provided by the LiCl-H_2O solution, while the $LiNO_3$-NH_3 and LiBr-H_2O solutions supply similar cooling. For the three solutions, higher salt concentration provides higher cooling effect. In this case, the solution inlet temperature is fixed, therefore the change in concentration implies higher subcooling of the solution and a higher pressure potential. A change in the inlet solution concentration of 3% leads to an increase in the chilling power of 62% for the LiBr-H_2O, 130% for the LiCl-H_2O and 92% for the $LiNO_3$-NH_3. This increase in the cooling capacity is obtained with a higher COP as shown in Fig. 11.

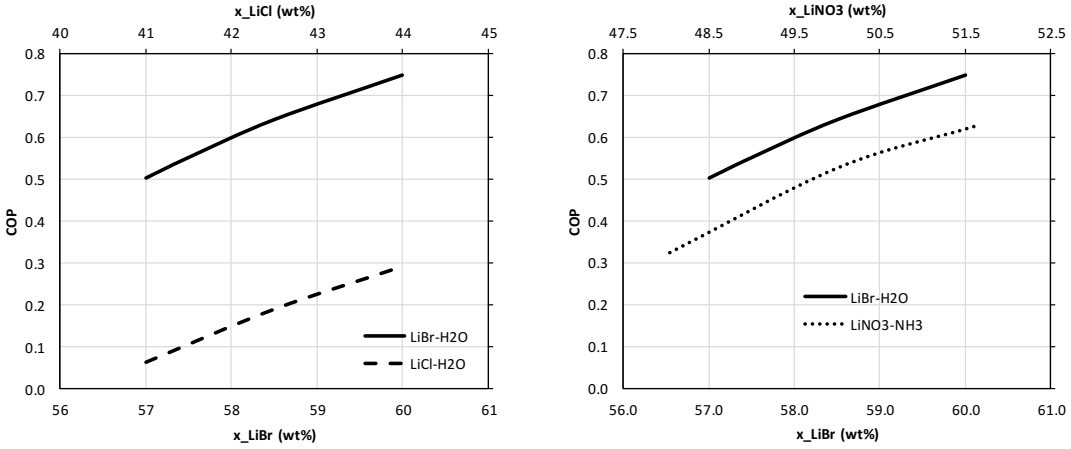

Fig. 11. Effect of solution concentration in the coefficient of performance of an absorption chiller working with a 5 cm long membrane absorber: LiCl-H_2O and LiBr-H_2O (a)(left); $LiNO_3$-NH_3 and LiBr-H_2O (b)(right).

The LiBr-H_2O provides the highest COP, while the LiCl-H_2O pair works with a poor performance (below 0.3). The $LiNO_3$-H_2O and LiBr-H_2O can provide similar cooling effects, but with a better COP in the second case. As a novelty of the present

paper, it is the first time that the COP of the chiller operating with the LiCl-H_2O and $LiNO_3$-NH_3 solutions in a membrane-based absorber is provided.

The final temperature in the desorber for the same cases is represented in Fig. 12 for the three solutions. The advantage of the new proposed working solutions is that they could work at lower desorber temperatures. The LiCl-H_2O solution, as shown in Fig. 12, could work with generation temperatures below 70 ºC. Nevertheless, in this operating condition, the COP will be equal to 0.3 producing a chilling effect of 3 W. The $LiNO_3$-H_2O can work also at lower temperatures than the LiBr-H_2O solution, but the difference is less pronounced. For example, if a cooling demand of 7 W is considered, this could be provided with a LiBr-H_2O system operating with an inlet concentration at the absorber of 59.25%, a COP equal to 0.7 and a final desorber temperature of 77.5 ºC. The $LiNO_3$-NH_3 will provide the same cooling effect working with a solution concentration of 50.25%, a COP equal to 0.55 and the final temperature in the desorber would be 74.5 ºC.

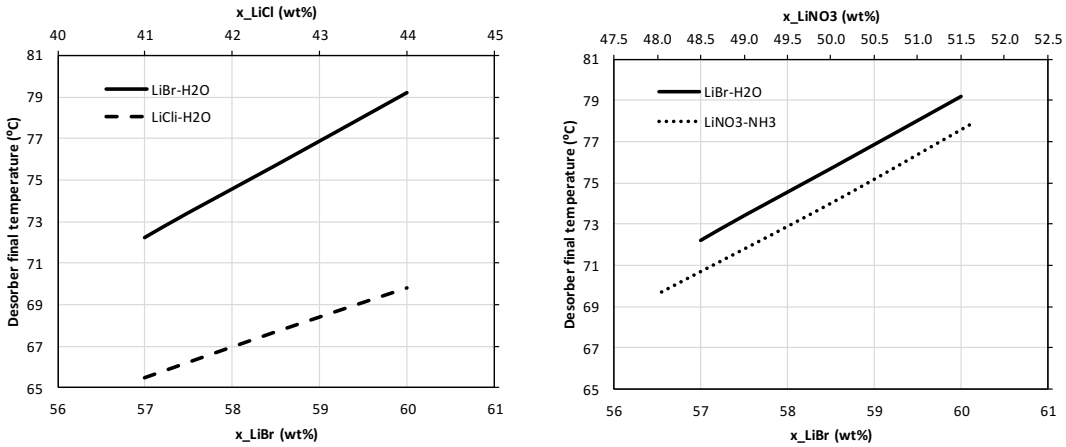

Fig. 12. Effect of solution concentration in the solution temperature at the outlet of the desorber of an absorption chiller working with a 5 cm long membrane absorber: LiCl-H_2O and LiBr-H_2O (a)(left); $LiNO_3$-NH_3 and LiBr-H_2O (b)(right).

The effect of varying the solution inlet temperature is shown in Fig. 13. As it is expected, the maximum cooling effect and COP are achieved at lower solution inlet temperatures because the solution would have a higher subcooling, increasing its capacity to absorb vapour. With a solution inlet temperature of 36 ºC, a cooling effect of 1.24 W can be obtained using the LiCl-H_2O solution (with a concentration equal to x_{LiCl} = 42.5%). In this case the COP will be 0.1. With the same inlet solution temperature, a LiBr-H_2O solution (at 58.5% concentration) will provide 5.74 W with a COP equal to 0.51. The $LiNO_3$-NH_3 at 50%, will provide 6 W with a COP of 0.42.

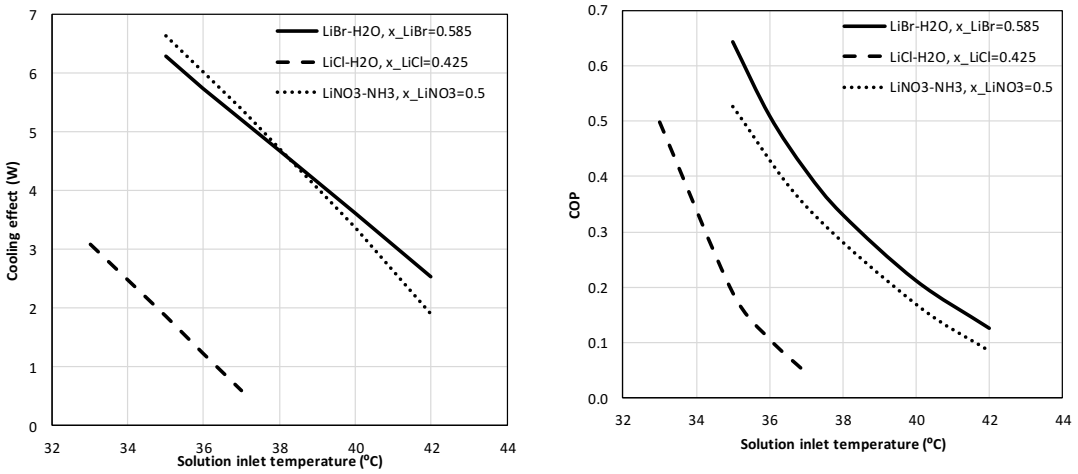

Fig. 13. Effect of the solution inlet temperature in the cooling effect (left) and coefficient of performance (right) of an absorption chiller working with a 5 cm long membrane absorber.

A comprehensive representation of the previous results is shown in Fig. 14 where the cooling effect as a function of the temperature of the heating source is represented. This figure can be used as a design tool to select one of the three solutions and, for each case, determine the working concentrations and need of cooling of the solution for a given cooling duty.

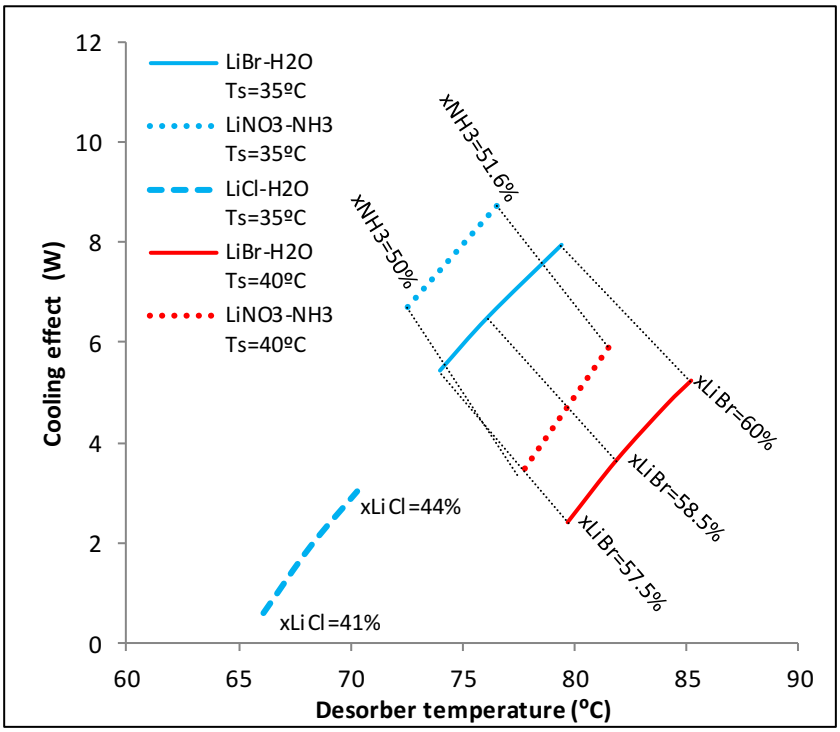

Fig. 14. Cooling effect comparison for a chiller operating with a microchannel membrane based absorber of 9.5 cm^3 in volume.

For example, a cooling effect of 3 W can be obtained using the LiCl-H_2O solution at x_{LiCl}=44%, entering the absorber at 35 ºC in a system fed with a heating medium around 70 ºC. To obtain the same cooling effect a LiBr-H_2O solution at 40 ºC and 58%

concentration will need a temperature in the desorber of 82 ºC, while the $LiNO_3$-NH_3 solution could work with a solution at 40 ºC and a concentration of 50%, in a system feeding the generator at around 77 ºC.

In the present work an absorber of 9.5 cm^3 is considered. Scaling to higher cooling powers is easily achieved by increasing the number of channels or stacking the required number of modules. In this way, a 1 kW system could be achieved, for example, with 8 adjacent modules of 150 channels each, or 4 modules with 300 channels.

To our best knowledge, this kind of results has not been reported before. It is the first time that information on the performance of a complete absorption chiller working with the three different solutions of this study (LiBr-H_2O, LiCl-H_2O and $LiNO_3$-NH_3) in a microchannel membrane-based absorber is provided.

4. Conclusions

In the present work, the simulation of the absorption process through a membrane in a microchannel absorber allowed the comparison of the alternative solutions LiCl-H_2O and $LiNO_3$-NH_3 with the conventional LiBr-H_2O working pair. This comparison has not been reported in the literature. In order to compare the performance of the LiBr-H_2O, LiCl-H_2O and $LiNO_3$-NH_3 solutions, the data referred to their thermodynamic and physical properties in the literature have been first exhaustively reviewed. In particular, an effort has been stressed on the calculation of the diffusion coefficient, which value determines in a great manner the mass transfer between the refrigerant and the solution. This has allowed the evaluation of the heat and mass transfer coefficients at different operating temperatures and concentrations.

The simulated performance of the LiBr-H_2O, LiCl-H_2O and $LiNO_3$-NH_3 solutions working in a membrane based process has shown that they can provide small-size absorbers in comparison to the conventional ones working with a falling film solution sheet. The cooling effect to absorber volume ratio has been used as a base of comparison. The highest value for this parameter is obtained using the $LiNO_3$-NH_3 pair. The LiCl-H_2O provides, in comparison, the lowest ratio.

Another novelty is the study of the membrane absorber in a complete absorption chiller for the three solutions. In this way, the cooling effect and coefficient of performance for different concentrations, cooling water temperatures and temperature of the heating source are estimated and an operational map for the three solutions has been drawn. These charts reveal that the highest cooling effect can be achieved with the $LiNO_3$-NH_3 solution, with lower temperatures in the desorber than the ones needed in the LiBr-H_2O system. Nevertheless, the system working with the LiBr-H_2O solution possesses the best COP. The maximum cooling effect is achieved at lower solution temperatures and higher salt concentrations. The lower temperatures are obtained in the desorber using the LiCl-H_2O solution, but with poor coefficient of performance and low cooling effect. As a novelty, the paper also provides criteria for the selection of the most

suitable solution for each application, depending on the available heat source and condensation temperature levels.

Acknowledgements

The financial support of this study by the Ministerio de Economía y Competitividad of Spain through the research grant DPI2017-83123-R is greatly appreciated.

References

[1] Parham K, Atikol U, Yari M, Agboola OP. Evaluation and Optimization of Single Stage Absorption Chiller Using (LiCl + H_2O) as the Working Pair. Adv. Mech. Eng. 2013; 5. doi: 10.1155/2013/683157.

[2] Sun J, Fu L, Zhang S. A review of working fluids of absorption cycles. Renew. Sust. Energ. Rev. 2012; 16: 1899-1906. doi:10.1016/j.rser.2012.01.011.

[3] Sarbu I, Sebarchievici C. General review of solar-powered closed sorption refrigeration systems. Energy Conv. Manag. 2015; 105: 403-422. doi: 10.1016/j.enconman.2015.07.084.

[4] Acuña A, Velazquez N, Cerezo J. Energy analysis of a diffusion absorption cooling system using lithium nitrate, sodium thiocyanate and water as absorbent substances and ammonia as the refrigerant. Appl. Therm. Eng. 2013; 51: 1273-1281. doi: 10.1016/j.applthermaleng.2012.10.046.

[5] Sun D-W. Comparison of the performances of NH_3-H_2O, NH_3-$LiNO_3$ and NH_3-NaSCN absorption refrigeration systems. Energy Conv. Manag. 1998; 39(5/6): 357-368. doi: 10.1016/S0196-8904(97)00027-7.

[6] Abdulateef JM, Sopian K, Alghoul MA. Optimum design for solar absorption refrigeration systems and comparison of the performances using ammonia-water, ammonia/lithium nitrate and ammonia-sodium thiocyanate solutions. Int. J. Mech. Mater. Eng. 2008; 3(1): 17-24.

[7] Venegas M, Izquierdo M, de Vega M, Lecuona A. Thermodynamic study of multistage absorption cycles using low temperature heat. Int. J. Energy Res. 2002; 26: 775-791. doi: 10.1002/er.815.

[8] Antonopoulos KA, Rogdakis ED. Performance of solar-driven ammonia-lithium nitrate and ammonia-sodium thiocyanate absorption systems operating as coolers or heat pumps in Athens. Appl. Therm. Eng. 1996; 16(2): 127-147. doi: 10.1016/1359-4311(95)00046-G.

[9] Ayala R, Heard CL, Holland FA. Ammonia/lithium nitrate absorption/ compression refrigeration cycle. Part II. Experimental. Appl. Therm. Eng. 1998; 18(8): 661-670. doi: 10.1016/S1359-4311(97)00077-X.

[10] Hernández-Magallanes JA, Domínguez-Inzunza LA, Gutiérrez-Urueta G, Soto P, Jiménez C, Rivera W. Experimental assessment of an absorption cooling system operating with the ammonia/lithium nitrate mixture. Energy. 2014; 78: 685-692. doi: 10.1016/j.energy.2014.10.058.

[11] Zamora M, Bourouis M, Coronas A, Vallés M. Pre-industrial development and experimental characterization of new air-cooled and water-cooled ammonia/lithium nitrate absorption chillers. Int. J. Refrig. 2014; 45: 189-197. doi: 10.1016/j.ijrefrig.2014.06.005.

[12] Zamora M, Bourouis, M, Coronas A, Vallés M. Part-load characteristics of a new ammonia/lithium nitrate absorption chiller. Int. J. Refrig. 2015; 56: 43-51. doi: 10.1016/j.ijrefrig.2014.11.005.

[13] Vasilescu C, Infante Ferreira C. Solar driven double-effect absorption cycles for sub-zero temperatures. Int. J. Refrig. 2014; 39: 86-94. doi: 10.1016/j.ijrefrig.2013.09.034.

[14] Wang JF, Gao GC, Chen GM. An improved absorption refrigeration cycle driven by unsteady thermal sources below 100 ºC. Int. J. Energy Res. 2000; 24(7): 633-640. doi: 10.1002/1099-114X(20000610)24:7<633::AID-ER618>3.0.CO;2-K.

[15] Barragán Reyes RM, Arellano Gómez VM, García-Gutiérrez A. Performance modelling of single and double absorption heat transformers. Curr. Appl. Phys. 2010; 10: S244-S248. doi: 10.1016/j.cap.2009.11.052.

[16] She X, Yin Y, Xu M, Zhang X. A novel low-grade heat-driven absorption refrigeration system with LiCl-H_2O and LiBr-H_2O working pairs. Int. J. Refrig. 2015; 58: 219-234. doi: 10.1016/j.ijrefrig.2015.06.016.

[17] El-Ghalban AR. Operational results of an intermittent absorption cooling unit. Int. J. Energy Res. 2002; 26: 825–835. doi: 10.1002/er.822.

[18] Gommed K, Grossman G, Ziegler F. Experimental Investigation of a LiCl-water Open Absorption System for Cooling and Dehumidification. J. Sol. Energy Eng. Trans.-ASME. 2004; 126: 710-715. doi: 10.1115/1.1643075.

[19] Garimella S, Determan MD, Meacham JM, Lee S, Ernst TC. Microchannel component technology for system-wide application in ammonia/water absorption heat pumps. Int. J. Refrig. 2011; 34: 1184-1196. doi: 10.1016/j.ijrefrig.2011.03.005.

[20] Ali AHH, Schwerdt P. Characteristics of the membrane utilized in a compact absorber for lithium bromide–water absorption chillers. Int. J. Refrig. 2009; 32: 1886-1896. doi: 10.1016/j.ijrefrig.2009.07.009.

[21] Asfand F, Bourouis M. A review of membrane contactors applied in absorption refrigeration systems. Renew. Sust. Energy Rev. 2015; 45: 173-191. doi: 10.1016/j.rser.2015.01.054.

[22] Chen J, Chang H, Chen S-R. Simulation study of a hybrid absorber-heat exchanger using hollow fiber membrane module for the ammonia-water absorption cycle. Int. J. Refrig. 2006; 29: 1043-1052. doi: 10.1016/j.ijrefrig.2006.02.002.

[23] Schaal F, Weimer T, Hasse H. Membrane Contactors for Absorption Refrigeration. International Sorption Heat Pump Conference, Seoul, Korea 2008.

[24] Ali AHH. Design of a compact absorber with a hydrophobic membrane contactor at the liquid-vapor interface for lithium bromide-water absorption chillers. Appl. Energy. 2010; 87: 1112-1121. doi: 10.1016/j.apenergy.2009.05.018.
[25] Yu D, Chung J, Moghaddam S. Parametric study of water vapour absorption into a constrained thin film of lithium bromide solution. Int. J. Heat Mass Transf. 2012; 55: 5687-5695. doi: 10.1016/j.ijheatmasstransfer.2012.05.064.
[26] Isfahani RN, Moghaddam S. Absorption characteristics of lithium bromide (LiBr) solution constrained by superhydrophobic nanofibrous structures. Int. J. Heat Mass Transf. 2013; 63: 82-90. doi: 10.1016 /j.ijheatmasstransfer.2013.03.053.
[27] Venegas M, de Vega M, García-Hernando N, Ruiz-Rivas U. A simple model to predict the performance of a H_2O-LiBr absorber operating with a microporous membrane. Energy. 2013; 96: 383-393. doi: 10.1016/j.energy.2015.12.059.
[28] Asfand F, Stiriba Y, Bourouis M. Performance evaluation of membrane-based absorbers employing H_2O/(LiBr+LiI+$LiNO_3$+LiCl) and H_2O/($LiNO_3$+KNO_3+$NaNO_3$) as working pairs in absorption cooling systems. Energy. 2016; 115: 781-790. doi: 10.1016/j.energy.2016.08.103.
[29] Lee P-S, Garimella SV. Thermally developing flow and heat transfer in rectangular microchannels of different aspect ratios. Int. J. Heat Mass Transf. 2006; 49: 3060-3067. doi: 10.1016/j.ijheatmasstransfer.2006.02.011.
[30] Shah RK, London AL. Laminar flow forced convection in ducts, in: a source book for compact heat exchanger analytical data. Advances in heat transfer. New York: Academic Press; 1978. Suppl. 1.
[31] Kim YJ, Joshi YK, Fedorov AG. An absorption based miniature heat pump system for electronics cooling. Int. J. Refrig. 2008; 31: 23-33. doi:10.1016/j.ijrefrig.2007.07.003.
[32] Asfand F, Stiriba Y, Bourouis M. Impact of the solution channel thickness while investigating the effect of membrane characteristics and operating conditions on the performance of water-LiBr membrane-based absorbers. Appl. Therm. Eng. 2016; 108: 866-877. doi: 10.1016/j.applthermaleng.2016.07.139.
[33] Taylor R, Krishna R. Multicomponent mass transfer. New York: John Wiley & Sons; 1993.
[34] Martínez L, Rodríguez-Maroto JM. Characterization of membrane distillation modules and analysis of mass flux enhancement by cannel spacers. J. Membr. Sci. 2006; 274: 123-137. doi: 10.1016/j.memsci.2005.07.045.
[35] Berdasco M, Coronas A, Vallès M. Theoretical and experimental study of the ammonia/water absorption process using a flat sheet membrane module. Appl. Therm. Eng. 2017, 124: 477-485. doi j.applthermaleng.2017.06.0271359-4311.
[36] Pátek J, Klomfar J. A computationally effective formulation of the thermodynamic properties of LiBr-H2O from 273 to 500 K over full composition range. Int. J. Refrig. 2006; 29: 566-578. doi: 10.1016 /j.ijrefrig.2005.10.007.

[37] DiGuilio RM, Lee RJ, Jeter SM, Teja AS. Properties of Lithium Bromide-Water Solutions at High Temperatures and Concentrations - I Thermal Conductivity. ASHRAE Trans., Paper 3380, RP-527 (1990) pp. 702-708.
[38] Lee RJ, DiGuilio RM, Jeter SM, Teja AS. Properties of Lithium Bromide-Water Solutions at High Temperatures and Concentrations - II Density and Viscosity. ASHRAE Trans., Paper 3381, RP-527 (1990) pp. 709-714.
[39] Kim KJ, Berman NS, Chau DSC, Wood BD. Absorption of water vapour into falling films of aqueous lithium bromide. Int. J. Refrig. 1995; 18(7): 486-494. doi: 10.1016/0140-7007(95)93787-K.
[40] Mittermaier M, Schulze P, Ziegler F. A numerical model for combined heat and mass transfer in a laminar liquid falling film with simplified hydrodynamics. Int. J. Heat Mass Transf. 2014; 70: 990-1002. doi: 10.1016/j.ijheatmasstransfer.2013.11.075.
[41] Pátek J, Klomfar J. Thermodynamic properties of the LiCl-H_2O system at vapor-liquid equilibrium from 273 K to 400 K. Int. J. Refrig. 2008; 31: 287-303. doi: 10.1016/j.ijrefrig.2007.05.003.
[42] Conde MR. Properties of aqueous solutions of lithium and calcium chlorides: formulations for use in air conditioning equipment design. Int. J. Therm. Sci. 2004; 43: 367-382. doi: 10.1016/j.ijthermalsci.2003.09.003.
[43] Conde M. Aqueous solutions of lithium and calcium chlorides: property formulations for use in air conditioning equipment design. M. Conde Engineering, Zurich, 2014.
[44] Bouazizi S, Nasr S. Concentration effects on aqueous lithium chloride solutions. Molecular dynamics simulations and x-ray scattering studies. J. Mol. Liq. 2014; 197: 77-83. doi: 10.1016/j.molliq.2014.04.018.
[45] Libotean S, Salavera D, Valles M, Esteve X, Coronas A. Vapor-Liquid Equilibrium of Ammonia + Lithium Nitrate + Water and Ammonia + Lithium Nitrate Solutions from (293.15 to 353.15) K. J. Chem. Eng. Data. 2007; 52 (3): 1050-1055. doi: 10.1021/je7000045.
[46] Libotean S, Martin A, Salavera D, Valles M, Esteve X, Coronas A. Vapor-Densities, Viscosities, and Heat Capacities of Ammonia + Lithium Nitrate and Ammonia + Lithium Nitrate + Water Solutions between (293.15 to 353.15) K. J. Chem. Eng. Data. 2008; 53(10): 2383-2388. doi: 10.1021/je8003035.
[47] Infante Ferreira CA. Vertical tubular absorbers for ammonia-salt absorption refrigeration. Laboratory for Refrigeration and Indoor Climate Technology, 1985.
[48] Kusaka R, Ban K, Nakamura Y, Shimokawa S. Diffusion of cations and solvent molecules in the concentrated $LiNO_3$-NH_3 system. J. Phys. Chem. 1987; 91(4): 985-987. doi: 10.1021/j100288a042.
[49] Herold KE, Radermacher E, Klein SA. Absorption Chillers and Heat Pumps. CRC Press. Boca Raton. 1996.

[50] Bellos E, Tzivanidis Ch, Antonopoulos KA. Exergetic and energetic comparison of LiCl-H_2O and LiBr-H_2O working pairs in a solar absorption cooling system. Energy Conv. Manag. 2016; 123: 453-461. doi: 10.1016/j.enconman.2016.06.068.
[51] Kim KJ, Ameel TA, Wood BD. Performance evaluations of LiCl and LiBr for absorber design applications in the open-cycle absorption refrigeration system. J. Sol. Energy Eng. Trans.-ASME. 1997; 119(2): 165-173. doi:10.1115/1.2887898.
[52] Gao Q, Lizarazo-Adarme J, Paul BK, Haapala KR. An economic and environmental assessment model for microchannel device manufacturing: part 2 - Application. J. Clean. Prod. 2016; 120: 146-156. doi: j.jclepro.2015.04.141.
[53] Leith S. Toward Low-Cost fabrication of microchannel process technologies – Cost modeling for manufacturing development. AIChE Annual Meeting High Throughput and Compact Processing Technologies. Salt Lake City, Utah, USA November, 2010.